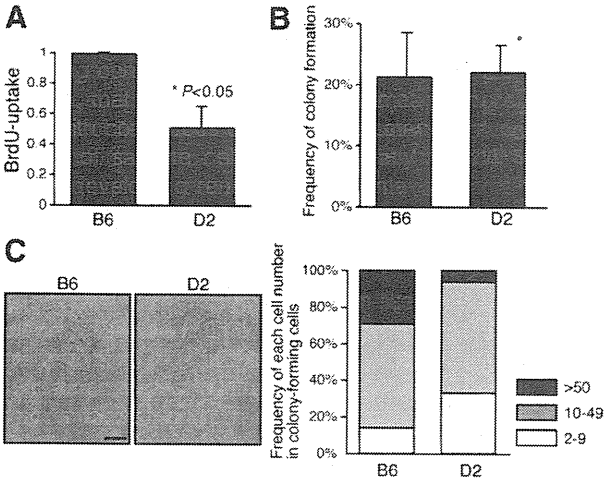

Figure 4. Satellite cells of DBA/2 strain show inferior BrdU uptake and colony-forming potential. **A:** BrdU uptake of primary myoblasts derived from C57BL/6 or DBA/2 satellite cells. The *y* axis shows the mean with SD of three independent experiments. $^{*}P < 0.05$ (Student's *t*-test). Frequency of colony formation by a single satellite cell derived from C57BL/6 or DBA/2 (**B**) and the size of single cell-derived colonies (**C**). The picture shows representative colonies of each strain. Colonies were categorized into three groups: >50 cells/well, 10 to 49 cells/well, and 2 to 9 cells/well. The *y* axis indicates the frequency (**B**) or percentage of each category (**C**) from three independent experiments. Scale bar = 100 μm.

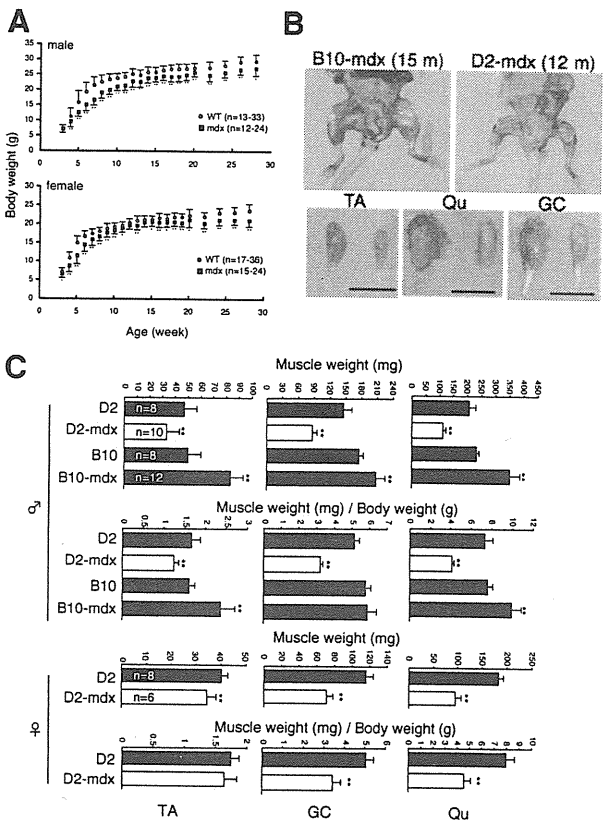

Figure 5. DBA/2-*mdx* mice show decreased body weight and remarkable muscle weight loss. **A:** Body weight of D2-*mdx* (closed squares) and their wild or heterozygous littermates (open circles) related to age. $^{*}P < 0.05$, $^{**}P < 0.01$ (Student's *t*-test) **B:** Photographs of hind limb muscles of male B10-*mdx* (15 months) and D2-*mdx* (12 months). Scale bar = 1 cm. **C:** TA, GC, and Qu muscle weights (mg) or per body weight (g) of 6-month-old mice. *x* axis shows the mean with SD. The numbers of muscles used in each study are shown in each graph. $^{*}P < 0.05$, $^{**}P < 0.01$.

because C57BL10-*mdx* mice already have dystrophic degeneration–regeneration cycles. Sadeh et al[25] also showed active regeneration cycles in rats that received weekly injections of bupivacaine for 6 months. They reported that there was lack of evidence for reduction or exhaustion of muscle fiber capacity to regenerate despite ongoing degeneration–regeneration over a period approximating one fourth of the rat life expectancy. These results indicate that the satellite cell pool was efficiently maintained for multiple degeneration–regeneration cycles in these animals, and that dystrophic mice exhibit less regeneration ability. However, DBA/2 showed significantly decreased numbers of myofibers and self-renewed satellite cells after only three injections of CTX.

The number of DBA/2 satellite cells in uninjured TA muscle is similar to that of C57BL/6. Although, the myofibers in DBA/2 were smaller than those in C57BL/6 2 weeks after one CTX injection (data not shown), the myofiber size and histological characteristics showed few significant differences between and DBA/2 and C57BL/6 4 weeks after a single CTX injection. These results suggest that the self-renewal ability of DBA/2 satellite cells is incomplete and that the exhaustion of muscle satellite cells leads to a decreased number of myofiber and loss of skeletal muscle weight. Nonmyogenic cells, for example, macrophages, also play important roles in skeletal muscle regeneration. However, dysfunction of macrophages leads to impaired regeneration after one CTX injection.[26,27] Furthermore, the remarkable regeneration deficit was not observed in DBA/2 4 weeks after one CTX injection in TA muscle. These results suggest that repeated injury is a suitable model to assess the long-term regeneration potential of skeletal muscle, and that the self-renewal ability of satellite cells is responsible at least in part for the result of repeatedly injured muscle in DBA/2.

Strain Differences of Muscle Regeneration Ability

C57BL/6, a strain akin to C57BL/10, is the most widely used strain for skeletal muscle regeneration studies. As shown in Figure 1, C57BL/6 has the best ability to regenerate skeletal muscle among the four inbred strains examined. An early study by Grounds and McGeachie[28] indicated a strain difference in skeletal muscle regeneration between BALB/c and Swiss SJL/J. They showed that superior and faster regeneration was observed in the Swiss SJL/J strain. The most outstanding phenotype of DBA/2 is the remarkable decrease of muscle weight compared with the three other inbred strains, including BALB/c. Intriguingly, DBA/2 mice have a shorter life span than C57BL/6.[29] In addition, it is reported that muscle weight loss is increased during aging (sarcopenia) in DBA/2 mice compared with C57BL/6.[30] The reason why the DBA/2 strain exhibits the loss of muscle weight is unknown, but our results imply a relationship between

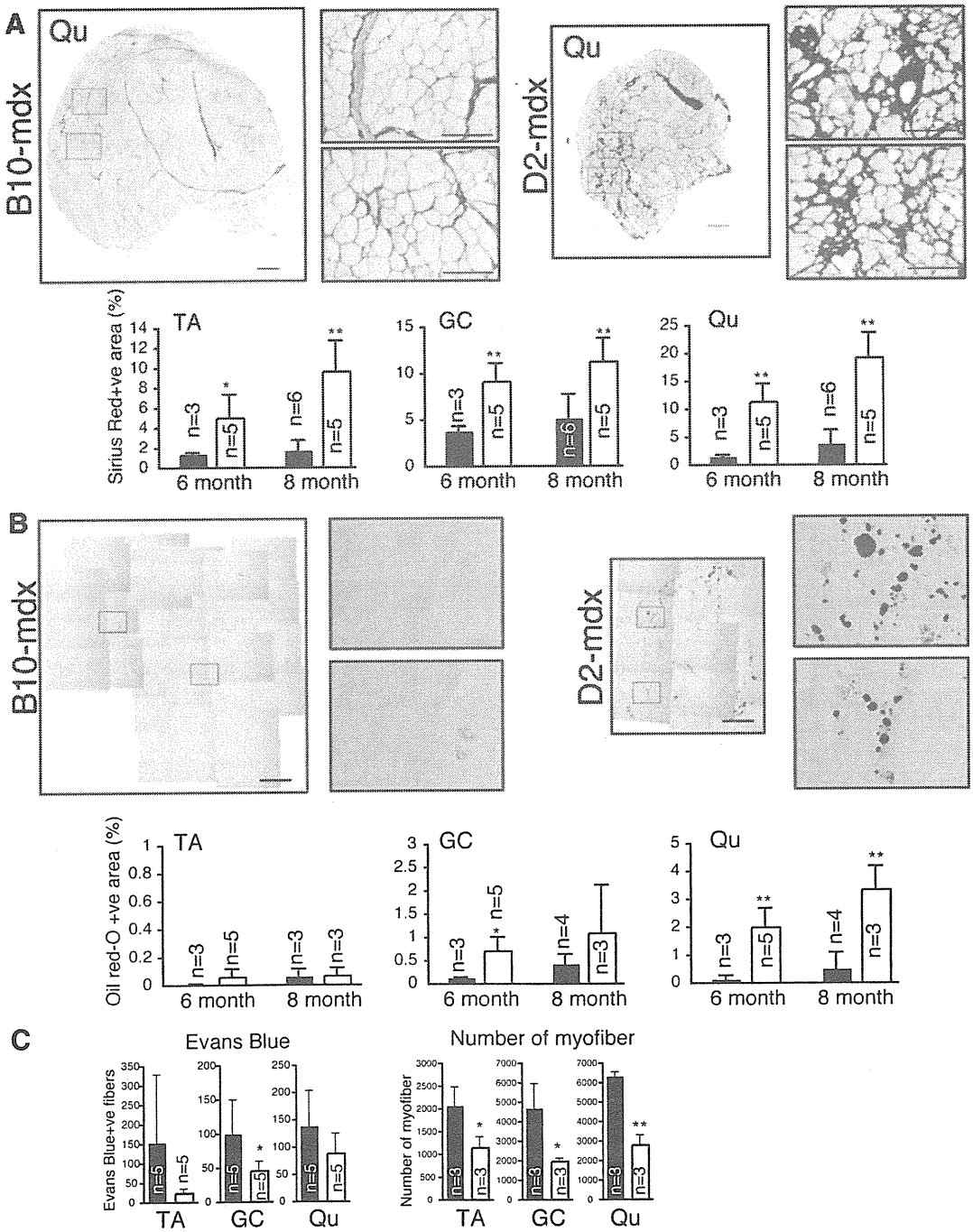

Figure 6. Histological analyses of DBA/2-*mdx* mice. Sirius red staining (**A**) and Oil red-O staining (**B**) of Qu muscle of 8-month-old B10-*mdx* and D2-*mdx* mice. The *y* axis indicates the mean percentage of Sirius Red- (**A**) or Oil red-O (**B**) -positive areas per section. The *x* axis indicates the age of mice. Black and white columns show the results for B10-*mdx* and D2-*mdx*, respectively. The numbers of mice used in each study are shown in each graph. **C:** The *y* axis indicates the mean number of Evans blue-positive or total myofibers of B10-*mdx* and D2-*mdx* at 8 months of age. $^{*}P < 0.05$, $^{**}P < 0.01$.

the impaired function of satellite cells and sarcopenia in DBA/2.

Heydemann et al[31] reported that γ-sarcoglycan-null mice with DBA/2 background showed decreased skeletal muscle weight, increased Evans Blue uptake, and a higher hydroxyproline concentration than C57BL/6, CD1, and 129 background null mice. Although they ruled out the voluntary activities of DBA/2, they did not discuss the cause of these results. Our results suggest that the low regeneration potential of DBA/2 leads to a severe skeletal muscle phenotype in various dystrophic mouse models.

The DBA/2J strain has been used in sarcopenia and γ-sarcoglycan-null mouse studies.[30,31] To exclude the possibility that DBA/2 substrain differences exist, we compared the BrdU uptake of primary myoblasts in DBA/2N (used in this study) and DBA/2J. Because we observed similar low BrdU uptakes by primary myoblasts in both DBA/2N and DBA/2J (data not shown), these

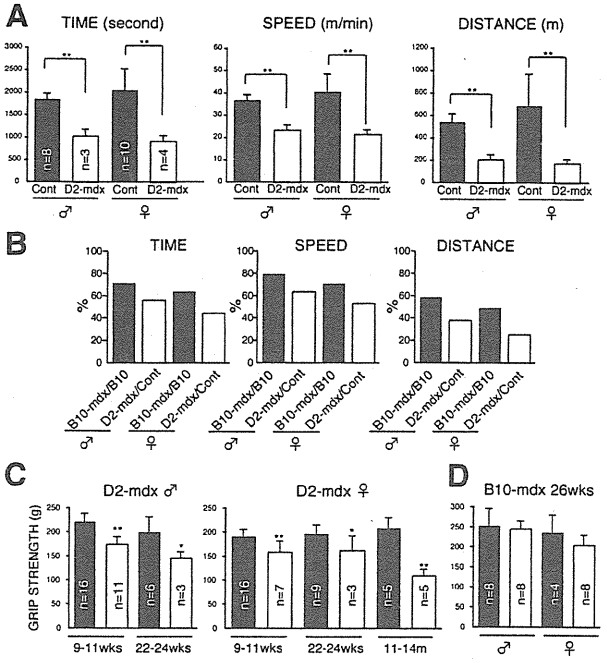

Figure 7. Comparison of muscle strength in DBA/2-*mdx* and B10-*mdx*. **A:** Treadmill running test of mice at 24 weeks old. Final time, speed, and distance were recorded and calculated for the individual performance score. The averages are shown with SD. Control indicates heterozygous or wild-type littermates of D2-*mdx*. The numbers of mice used in each study are shown in each graph. $^{*}P < 0.05$, $^{**}P < 0.01$. **B:** Comparison of C57BL/10-*mdx* and DBA/2-*mdx* in treadmill running test. The *y* axis indicates the percentage of *mdx* per control value. The numbers of male C57BL/10, male C57BL/10-*mdx*, female C57BL/10, and female C57BL/10-*mdx* are 4, 4, 4, and 8, respectively. Grip strength test of D2-*mdx* (**C**) or B10-*mdx* (**D**). Black and white columns indicate the results for *mdx* or control mice, respectively. The *y* axis indicates the average score of each mouse with SD. The *x* axis shows the ages of mice. The number in the each graph indicates the number of mice taking this test. $^{*}P < 0.05$, $^{**}P < 0.01$.

results suggest that lower muscle regeneration is common to the DBA/2 strain.

Stem (Satellite) Cell Function and Mouse Strains

As mentioned above, some previous reports indicated different responses in skeletal muscle regeneration among inbred strains of mice. However, to our knowledge, this is the first evidence that there is an intrinsic difference in satellite cells among inbred mice. The exact relationship between *in vitro* and *in vivo* results of satellite cells is not clear. However, low or slow proliferation of satellite cells might explain the decreased muscle weight and slow regeneration after a single injury in DBA/2 in comparison with C57BL/6 and B6D2F1, which showed increased muscle weight in their TA muscle (Figure 2A). It is unlikely that telomere erosion contributes to the *in vitro* and *in vivo* results of DBA/2 satellite cells because DBA/2 mice have longer telomeres than C57BL/6 mice.[32]

Recently Kuang et al[33] reported that satellite cells are a heterogeneous population of stem cells (satellite stem cells) and committed progenitor cells, and that they can be distinguished from others by Myf5 expression. They showed that Myf5-negative (satellite stem) cells self-renewed three times more frequently than Myf-5-positive (progenitor) cells *in vivo*. Schultz and Lipton[34] first described the heterogeneity of satellite cells by the different colony sizes of each satellite cell and found decreased colony sizes in aging muscle in the rat. Although it was not determined whether satellite stem cells form a large-colonies or not *in vitro*, our results showed that mice having low self-renewing satellite cells (DBA/2) exhibit smaller colony formations than mice having high self-renewing satellite cells (C57BL/6). These results suggest that satellite stem cells may form larger colonies *in vitro*.

In contrast to satellite cells, a highly strain-dependent function of hematopoietic stem cells was reported.[35] Chen et al[36] reported that DBA/2 showed a decline in primitive hematopoietic stem cell function with age, but that it increased with age in C57BL/6 in a *vivo* transplantation study. Recombinant inbred mice, named BXD strains, are available. Using BXD, Liang et al[37] identified latexin as affecting the size of the hematopoietic stem cell population in mice. A similar approach might lead to the discovery of key genes that affect the properties of satellite cells.

DBA/2-mdx *as Model for DMD*

Mdx was discovered a quarter of a century ago.[5] In 1989, the *mdx* mutation, a C to T transition within exon 23, was identified in the dystrophin gene on the X chromosome.[38] Nearly all *mdx* colonies are maintained as homozygous inbred lines; in addition, the difficulty of point mutation typing might impede the effect of genetic background on *mdx* phenotype. However, Amalfitano and Chamberlain[16] reported a rapid and simple typing strategy, and we established DBA/2-*mdx* following their protocol. C57BL/10-*mdx* mice have played central roles in a vast array of pathological, clinical, and physiological studies as a model for DMD. However, they do not reflect human pathology in some aspects, including little fat and fibrosis accumulation, no loss of myofiber numbers, and muscle weight. Recently, Gargioli et al[39] showed that the advanced stage of dystrophy including sclerosis precluded treatment by stem cell therapy. Therefore, assessment of therapeutic effect in more severe disease conditions is needed.

In marked contrast to the severe phenotype observed in DMD, early studies using C57BL/10-*mdx* concluded that they do not show obvious functional disability.[5,7] However, some later reports indicated functional differences between C57BL/10-*mdx* and control mice.[40–43] As shown in Figure 7, C57BL/6-*mdx* also showed muscle weakness in the treadmill test. However, the muscle weakness of DBA/2-*mdx* is more remarkable than that of C57BL/10-*mdx*. Therefore, DBA/2-*mdx* is a more appropriate model to assess skeletal muscle function after therapeutic treatment.

Chamberlain et al[44] reported that the average life spans of female and male C57BL/10-*mdx* mice were 22.5 and 21.5 months, respectively. Pastoret et al[8] also reported that C57BL/10-*mdx* mice have short life spans and that C57BL/10-*mdx* older than 78 weeks exhibit progressive weakness. We have not determined the life span of DBA/2-*mdx*, but it will be clarified in the future. Intrigu-

ingly, Chamberlain et al[44] observed the appearance of rhabdomyosarcoma-like tumors in C57BL/10-*mdx*. They speculate that the lifelong continuous myofiber degeneration and regeneration that characterize this animal model are associated with continuous and massive activation and proliferation of satellite cells, which greatly increase the chance of developing random and spontaneous mutations. To date, we have observed tumors in C57BL/10-*mdx* but not in DBA/2-*mdx*. This observation supports their speculations.

The reasons why *mdx* mice do not show the human-like pathology have been investigated. One reason for the difference between DMD and *mdx* is explained by the presence of utrophin, a homolog of dystrophin. Utrophin is located in the neuromuscular junction in normal muscle. In dystrophic muscle, utrophin is up-regulated in the sarcolemma and compensates for dystrophin function. As shown in Figure 6, the results of Evans blue uptake in DBA/2-*mdx* indicated that the degeneration of myofiber was not accelerated, but that the regeneration potential was inferior. These results clearly indicate that not only utrophin expression but also regeneration potential, perhaps a satellite cell function, directly leads to the pathological condition. The identification of genes that determine the DBA/2 phenotype will provide new therapeutic strategies for the treatment of muscular dystrophy.

Acknowledgment

We thank Katherine Ono for reading this manuscript.

References

1. Koenig M, Monaco AP, Kunkel LM: The complete sequence of dystrophin predicts a rod-shaped cytoskeletal protein. Cell 1988, 53:219–228
2. Suzuki A, Yoshida M, Hayashi K, Mizuno Y, Hagiwara Y, Ozawa E: Molecular organization at the glycoprotein-complex-binding site of dystrophin. Three dystrophin-associated proteins bind directly to the carboxy-terminal portion of dystrophin. Eur J Biochem 1994, 220:283–292
3. Ervasti JM, Campbell KP: A role for the dystrophin-glycoprotein complex as a transmembrane linker between laminin and actin. J Cell Biol 1993, 122:809–823
4. Carpenter S, Karpati G: Disease of skeletal muscle. Edited by S Carpenter, G Karpati. New York, Oxford University Press, Inc., 2001, pp. 373–524
5. Bulfield G, Siller WG, Wight PA, Moore KJ: X chromosome-linked muscular dystrophy (mdx) in the mouse. Proc Natl Acad Sci USA 1984, 81:1189–1192
6. Stedman HH, Sweeney HL, Shrager JB, Maguire HC, Panettieri RA, Petrof B, Narusawa M, Leferovich JM, Sladky JT, Kelly AM: The mdx mouse diaphragm reproduces the degenerative changes of Duchenne muscular dystrophy. Nature 1991, 352:536–539
7. Tanabe Y, Esaki K, Nomura T: Skeletal muscle pathology in X chromosome-linked muscular dystrophy (mdx) mouse. Acta Neuropathol 1986, 69:91–95
8. Pastoret C, Sebille A: mdx mice show progressive weakness and muscle deterioration with age. J Neurol Sci 1995, 129:97–105
9. Deconinck AE, Rafael JA, Skinner JA, Brown SC, Potter AC, Metzinger L, Watt DJ, Dickson JG, Tinsley JM, Davies KE: Utrophin-dystrophin-deficient mice as a model for Duchenne muscular dystrophy. Cell 1997, 90:717–727
10. Grady RM, Teng H, Nichol MC, Cunningham JC, Wilkinson RS, Sanes JR: Skeletal and cardiac myopathies in mice lacking utrophin and dystrophin: a model for Duchenne muscular dystrophy. Cell 1997, 90:729–738
11. Bischoff R: Analysis of muscle regeneration using single myofibers in culture. Med Sci Sports Exerc 1989, 21:S164–172
12. Mauro A: Satellite cell of skeletal muscle fibers. J Biophys Biochem Cytol 1961, 9:493–495
13. Schultz E, Gibson MC, Champion T: Satellite cells are mitotically quiescent in mature mouse muscle: an EM and radioautographic study. J Exp Zool 1978, 206:451–456
14. Collins CA, Olsen I, Zammit PS, Heslop L, Petrie A, Partridge TA, Morgan JE: Stem cell function, self-renewal, and behavioral heterogeneity of cells from the adult muscle satellite cell niche. Cell 2005, 122:289–301
15. Luz MA, Marques MJ, Santo Neto H: Impaired regeneration of dystrophin-deficient muscle fibers is caused by exhaustion of myogenic cells. Braz J Med Biol Res 2002, 35:691–695
16. Amalfitano A, Chamberlain JS: The mdx-amplification-resistant mutation system assay, a simple and rapid polymerase chain reaction-based detection of the mdx allele. Muscle Nerve 1996, 19:1549–1553
17. Fukada S, Yamamoto Y, Segawa M, Sakamoto K, Nakajima M, Sato M, Morikawa D, Uezumi A, Miyagoe-Suzuki Y, Takeda S, Tsujikawa K, Yamamoto H: CD90-positive cells, an additional cell population, produce laminin alpha2 upon transplantation to dy(3k)/dy(3k) mice. Exp Cell Res 2008, 314:193–203
18. Fukada S, Higuchi S, Segawa M, Koda K, Yamamoto Y, Tsujikawa K, Kohama Y, Uezumi A, Imamura M, Miyagoe-Suzuki Y, Takeda S, Yamamoto H: Purification and cell-surface marker characterization of quiescent satellite cells from murine skeletal muscle by a novel monoclonal antibody. Exp Cell Res 2004, 296:245–255
19. Matsuda R, Nishikawa A, Tanaka H: Visualization of dystrophic muscle fibers in mdx mouse by vital staining with Evans blue: evidence of apoptosis in dystrophin-deficient muscle. J Biochem 1995, 118:959–964
20. Handschin C, Chin S, Li P, Liu F, Maratos-Flier E, Lebrasseur NK, Yan Z, Spiegelman BM: Skeletal muscle fiber-type switching, exercise intolerance, and myopathy in PGC-1alpha muscle-specific knock-out animals. J Biol Chem 2007, 282:30014–30021
21. Seale P, Sabourin LA, Girgis-Gabardo A, Mansouri A, Gruss P, Rudnicki MA: Pax7 is required for the specification of myogenic satellite cells. Cell 2000, 102:777–786
22. Connolly AM, Keeling RM, Mehta S, Pestronk A, Sanes JR: Three mouse models of muscular dystrophy: the natural history of strength and fatigue in dystrophin-, dystrophin/utrophin-, and laminin alpha2-deficient mice. Neuromuscul Disord 2001, 11:703–712
23. Charge SB, Rudnicki MA: Cellular and molecular regulation of muscle regeneration. Physiol Rev 2004, 84:209–238
24. Sacco A, Doyonnas R, Kraft P, Vitorovic S, Blau HM: Self-renewal and expansion of single transplanted muscle stem cells. Nature 2008, 456:502–506
25. Sadeh M, Czyewski K, Stern LZ: Chronic myopathy induced by repeated bupivacaine injections. J Neurol Sci 1985, 67:229–238
26. Arnold L, Henry A, Poron F, Baba-Am Y, van Rooijen N, Plonquet A, Gherardi RK, Chazaud B: Inflammatory monocytes recruited after skeletal muscle injury switch into anti-inflammatory macrophages to support myogenesis. J Exp Med 2007, 204:1057–1069
27. Segawa M, Fukada S, Yamamoto Y, Yahagi H, Kanematsu M, Sato M, Ito T, Uezumi A, Hayashi S, Miyagoe-Suzuki Y, Takeda S, Tsujikawa K, Yamamoto H: Suppression of macrophage functions impairs skeletal muscle regeneration with severe fibrosis. Exp Cell Res 2008, 314:3232–3244
28. Grounds MD, McGeachie JK: A comparison of muscle precursor replication in crush-injured skeletal muscle of Swiss and BALBc mice. Cell Tissue Res 1989, 255:385–391
29. Gelman R, Watson A, Bronson R, Yunis E: Murine chromosomal regions correlated with longevity. Genetics 1988, 118:693–704
30. Lionikas A, Blizard DA, Vandenbergh DJ, Stout JT, Vogler GP, McClearn GE, Larsson L: Genetic determinants of weight of fast- and slow-twitch skeletal muscles in old mice. Mamm Genome 2006, 17:615–628
31. Heydemann A, Huber JM, Demonbreun A, Hadhazy M, McNally EM: Genetic background influences muscular dystrophy. Neuromuscul Disord 2005, 15:601–609
32. Manning EL, Crossland J, Dewey MJ, Van Zant G: Influences of

inbreeding and genetics on telomere length in mice. Mamm Genome 2002, 13:234–238
33. Kuang S, Kuroda K, Le Grand F, Rudnicki MA: Asymmetric self-renewal and commitment of satellite stem cells in muscle. Cell 2007, 129:999–1010
34. Schultz E, Lipton BH: Skeletal muscle satellite cells: changes in proliferation potential as a function of age. Mech Ageing Dev 1982, 20:377–383
35. Dykstra B, de Haan G: Hematopoietic stem cell aging and self-renewal. Cell Tissue Res 2008, 331:91–101
36. Chen J, Astle CM, Harrison DE: Genetic regulation of primitive hematopoietic stem cell senescence. Exp Hematol 2000, 28:442–450
37. Liang Y, Jansen M, Aronow B, Geiger H, Van Zant G: The quantitative trait gene latexin influences the size of the hematopoietic stem cell population in mice. Nat Genet 2007, 39:178–188
38. Sicinski P, Geng Y, Ryder-Cook AS, Barnard EA, Darlison MG, Barnard PJ: The molecular basis of muscular dystrophy in the mdx mouse: a point mutation. Science 1989, 244:1578–1580
39. Gargioli C, Coletta M, De Grandis F, Cannata SM, Cossu G: PlGF-MMP-9-expressing cells restore microcirculation and efficacy of cell therapy in aged dystrophic muscle. Nat Med 2008, 14:973–978
40. Muntoni F, Mateddu A, Marchei F, Clerk A, Serra G: Muscular weakness in the mdx mouse. J Neurol Sci 1993, 120:71–77
41. Hara H, Nolan PM, Scott MO, Bucan M, Wakayama Y, Fischbeck KH: Running endurance abnormality in mdx mice. Muscle Nerve 2002, 25:207–211
42. Carter GT, Wineinger MA, Walsh SA, Horasek SJ, Abresch RT, Fowler WM, Jr.: Effect of voluntary wheel-running exercise on muscles of the mdx mouse, Neuromuscul Disord 1995, 5:323–332
43. Lynch GS, Hinkle RT, Chamberlain JS, Brooks SV, Faulkner JA: Force and power output of fast and slow skeletal muscles from mdx mice 6–28 months old. J Physiol 2001, 535:591–600
44. Chamberlain JS, Metzger J, Reyes M, Townsend D, Faulkner JA: Dystrophin-deficient mdx mice display a reduced life span and are susceptible to spontaneous rhabdomyosarcoma. FASEB J 2007, 21:2195–2204

Acta Neuropathol (2010) 120:537–543
DOI 10.1007/s00401-010-0732-8

CASE REPORT

High-density areas on muscle CT in childhood-onset Pompe disease are caused by excess calcium accumulation

Keiko Ishigaki · Satomi Mitsuhashi · Ryohei Kuwatsuru · Terumi Murakami · Keiko Shishikura · Haruko Suzuki · Yoshito Hirayama · Ikuya Nonaka · Makiko Osawa

Received: 16 May 2010 / Revised: 15 July 2010 / Accepted: 24 July 2010 / Published online: 3 August 2010

Abstract We report two patients with childhood-onset Pompe disease showing striking changes with high-density areas on skeletal muscle CT, not seen in adult- or infantile-onset forms of this disease. While the anterior compartment of the thigh muscles was less affected in the adult-onset form, the rectus femoris and tibial muscles were preferentially involved from the early stage in the childhood-onset form of Pompe disease. The high-density areas became increasingly diffuse with disease progression, producing a marbled pattern and ultimately resulting in homogeneous high density and muscle atrophy. Muscle biopsy specimens from the high-density areas showed striking vacuolar changes with many dense globular bodies in lysosomes. High calcium signals were identified by X-ray microanalysis using energy-dispersive X-ray spectroscopy in these areas. Excess calcium accumulation in the vacuoles was also confirmed with the glyoxal-bis(2-hydroxyanil) (GBHA) staining. The high density on CT was slightly reduced together with clinical improvement after enzyme replacement therapy in patient 2. Our data demonstrate that in childhood-onset Pompe disease, high-density areas on skeletal muscle CT images are due to the accumulation of calcium in dense globular bodies formed by a chronic degenerative process affecting autophagic vacuoles.

Keywords Pompe disease · Childhood onset · High muscle CT density · Excess calcium accumulation · Enzyme replacement therapy

K. Ishigaki (✉) · T. Murakami · K. Shishikura · H. Suzuki · Y. Hirayama · M. Osawa
Department of Pediatrics, Tokyo Women's Medical University, School of Medicine, 8-1 Kawada-cho, Shinjuku-ku, Tokyo 162-8666, Japan
e-mail: keishi@ped.twmu.ac.jp

S. Mitsuhashi · I. Nonaka
National Center of Neurology and Psychiatry, Tokyo, Japan

R. Kuwatsuru
Department of Radiology, Tokyo Women's Medical University, School of Medicine, Tokyo, Japan

R. Kuwatsuru
Department of Radiology, Juntendo University, Faculty of Medicine, Tokyo, Japan

Introduction

Pompe disease is an autosomal recessively inherited disorder caused by a deficiency of the lysosomal enzyme acid alpha-glucosidase. It is classified into two major phenotypes, the infantile and late-onset forms, based on the time of disease onset [9]. The infantile form, originally described by Pompe, exhibits a rapidly progressive course characterized by prominent cardiomegaly, hepatomegaly, muscle weakness and hypotonia, and death before age 1 year. Late-onset Pompe disease is subdivided into childhood- and adult-onset forms. The childhood form usually presents with muscle weakness resembling that of progressive muscular dystrophy and is rarely associated with cardiomyopathy. Adult-onset Pompe disease is characterized by slowly progressive limb-girdle myopathy presenting as late as the second to sixth decade.

Computerized tomographic (CT) scanning of skeletal muscles is widely used for differential diagnosis or assessment of the progression of neuromuscular disorders [3, 12, 14]. The skeletal muscle CT abnormalities in adult-onset Pompe disease were reported to be atrophic, moth-eaten and washed-out changes in the paraspinal muscles [4]

and the vastus muscles of the thigh [5], and showed a pattern mimicking facioscapulohumeral dystrophy [10]. However, no report has summarized muscle CT findings in the childhood form. We previously reported a patient with childhood-onset Pompe disease showing high-density areas on CT in severely affected skeletal muscles [1]. Muscle biopsy of these high-density areas revealed pronounced vacuolar changes, while biopsy specimens from normal density areas had an essentially normal appearance. The second patient (patient 2) showed a very similar CT pattern, with high-density areas in the thigh and calf muscles, but no atrophic changes. In this study, we followed up CT changes in both the density and the volume of affected muscles in these two patients with age. We also determined whether the high-density areas improved with enzyme replacement therapy (ERT). Although the high-density areas on CT were associated with advanced vacuolar changes in muscle biopsy specimens, the precise mechanism whereby such changes were induced remains unknown. To clarify how CT density varies in the muscles of patients with Pompe disease, we analyzed this feature in the affected muscles.

Methods

Patients

Patient 1, previously reported elsewhere [1], was a 13-year-old boy at his first admission to our hospital. He had noticed muscle weakness and leg pain and severe headache upon awakening in the morning around 10 years of age. He had moderate muscle weakness only in the neck and trunk, without organomegaly. The characteristic histological findings and extremely low acid alpha-glucosidase activity (0.3 nmol 4 MU/mg/30 min, control: 7.3 ± 2.2) in biopsied muscle allowed a definitive diagnosis of Pompe disease. His genotype reflected compound heterozygous mutations, p.R600C and p.M439K, the former reportedly being common in Japanese patients. In his second decade, he suffered from repeated episodes of pneumothorax and respiratory infection. At age 19 years, non-invasive ventilation was necessitated by sudden aggravation of respiratory failure. He began ERT at 28 years but with no significant improvement and died of pneumonia at 29 years of age after 1 year treatment.

Patient 2 was an 11-year 3-month-old boy. At age 2 years, nasal voice became marked. He was apparently clumsy as compared with other children. At age 3 years, serum CK elevation to approximately 700 IU/l was detected incidentally during preoperative examination for nasopharyngeal incompetence. At age 5 years, he was diagnosed as having Pompe disease based on muscle biopsy findings and extremely low acid alpha-glucosidase activity, only 0.2 nmol 4 MU/mg/30 min (control: 7.3 ± 2.2). He had compound heterozygous missense mutations, p.S619R and p.E579K, which have already been reported. At 10 years and 3 months of age, International Charitable Access Program (ICAP) support allowed him to start ERT. At baseline, he could not jump and needed handrails to climb stairs. He was positive for Gowers' maneuver, and also had a waddling gait. He had mild respiratory failure and mild cardiac hypertrophy. ERT was initiated at a basic dosage of 20 mg/kg. Six months after starting ERT, his respiratory and motor functions were markedly improved.

Bone density was normal with normal renal function. Serum calcium levels and urine calcium to creatinine ratios (Ca/Cr) were within normal limits, measuring 8.8 mg/dl (normal 8.5–9.9) and 0.04 mg/mg (normal < 0.20) in patient 1 and 9.4 mg/dl and 0.02 mg/mg in patient 2, respectively. Serum phosphate and magnesium levels were also within normal limits, measuring 3.9 mg/dl (normal 2.5–4.5 mg/dl) and 1.5 mEq/l (normal 1.2–2.0) in patient 1 and 4.5 mg/dl and 1.5 mEq/l in patient 2, respectively. None of the patients had any abnormal symptoms of calcium metabolism. There was no clinical difference between our patients and others with the childhood form: all had proximal dominant progressive muscular weakness, respiratory dysfunction and slightly elevated CK levels.

Skeletal muscle CT scans

Skeletal muscle CT scans were obtained at seven levels, i.e., shoulder, mid-upper arm, mid-forearm, 3rd lumbar vertebra, pelvic girdle, mid-thigh and mid-calf (Hitachi CT 600 scanner, CT W-200, GE Highspeed Advantage SG, and Toshiba Aquilion 4 Detector). The scanning conditions, identical at all times, were 120 kVp, 150 mA and 0.5 ms. The CT number setting in Hounsfield units (HU) gives water a value of zero, air a value of −1,000 and bone a value of +1,000. The CT imaging should be displayed in the grey scales by adjusting window level (WL) and window width (WW) depending on target organs. The WW switch selects the range of absorption values that determine black and white on the display. The WL control enables the center of the range selected by the WW switch to be set at any desired point in the system's scale between −1,000 and +1,000. The earlier scans were obtained at a WL of 25 HU and WW of 225 HU using a Hitachi CT 600 scanner to evaluate skeletal muscles, while the more recent scans were obtained at WL 30–45 HU and WW 300–350 HU with more advanced CT scanners. Patient 1 was assessed at age 13, 22 and 29, and patient 2 at 5 and 10 years of age.

We also examined muscle CT on two patients with the infantile-onset, three with adult-onset forms and a 10-year-old girl with McArdle disease under the same conditions for comparison.

Morphological analysis

Biopsy specimens were taken from the rectus femoris, which showed high-density areas on CT, in both patients and from the vastus lateralis showing normal density in patient 1 at age 13 years (Fig. 5a). As a disease control, we selected two representative muscle biopsies from a patient with the infantile-onset form and two from another with the adult-onset form. Staining, including hematoxylin and eosin (HE) stain and Periodic acid-Schiff (PAS) stain, was performed by standard procedures. We also applied glyoxal-bis(2-hydroxyanil) (GBHA) staining to demonstrate insoluble red precipitates of calcium (Ca)–GBHA complexes in the muscle biopsy specimens. McArdle disease has abnormal glycogen metabolism but with small amount of glycogen accumulation and absent autophagic phenomenon. To confirm whether abnormal glycogen metabolism itself induces calcium accumulation in muscle fibers, we selected a 10-year-old patient with the McArdle disease as a disease control, and 20 normal muscles as healthy controls.

X-ray microanalysis (S-5200 ultra resolution scanning electron microscope: HITACHI)

The rectus femoris muscle was fixed in phosphate-buffered 2.5% glutaraldehyde, post-fixed in 1.5% osmium tetroxide and then embedded in epoxy resin employing a standard procedure. The sample was sectioned at approximately 0.1 μm and analyzed at 20 kV with an S-5200 ultra resolution scanning electron microscope (HITACHI) using the energy-dispersive X-ray spectroscopy (EDX) method. Samples from patients with juvenile dermatomyositis and Duchenne muscular dystrophy were analyzed for comparison.

Results

Skeletal muscle images

Both patients with the childhood-onset form specifically showed high-density areas on CT in the rectus femoris and tibialis anterior muscles from the early stage (Figs. 1a–c, 2a, b). The CT number (attenuation) for the high-density areas was approximately 130 HU, while these were in the 30–40 HU range in healthy controls. Even in the areas with near-normal density, CT numbers were increased to 70–80 HU in both patients. The skeletal muscle CT numbers in the patient with McArdle disease were slightly increased to 50–60 HU in all areas examined.

In patient 1 at 13 years of age, high-density areas were localized in the rectus femoris, as well as small portions of the adductor magnus and anterior tibialis muscles (Fig. 1b, c). The high-density areas became more diffuse with age, resulting in a marbled pattern but neither showed moth-eaten nor washed-out changes (Fig. 1e, f). Ultimately, most of his thigh and calf muscles showed homogeneous high density with marked volume loss (Fig. 1h, i). The paraspinal and iliopsoas muscles were also affected but there were no high-density areas (Fig. 1g).

In patient 2 at age 5 years, the rectus femoris muscle was mildly affected and high-density areas were detectable in the tibialis anterior and peroneal muscles (Fig. 2a, b). At 10 years of age, high-density areas became evident in the rectus femoris and also appeared in the vastus lateralis and gracilis muscles (Fig. 2c, d). He showed marked improvement of motor and respiratory functions 3 months after starting ERT. He could jump and climb stairs unaided. The CT numbers, of which the maximum had been 138 HU and the minimum 88 HU (138/88) at the beginning of ERT (Fig. 2c, d), improved slightly to 100/64 HU after

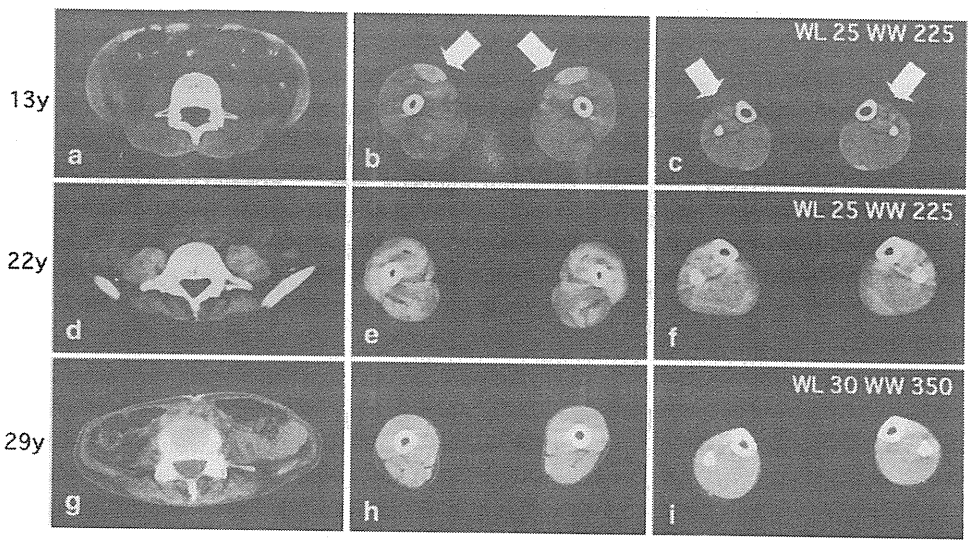

Fig. 1 Skeletal muscle CT scans in patient 1 at 13 years (**a–c**), 22 years (**d–f**) and 29 years (**g–i**) of age. Note high-density areas (*arrows*) in rectus femoris (**b**) and milder findings in the tibialis anterior (**c**) muscles, relatively sparing the posterior compartment of the thigh and calf muscles. As the high-density areas became more diffuse, a marbled pattern (**e**, **f**) appeared and eventually involved all leg muscles (**h**, **i**). Paraspinal muscles are also involved but do not show high-density areas (**a**, **d**, **g**). *WL* window level, *WW* window width of CT scanning

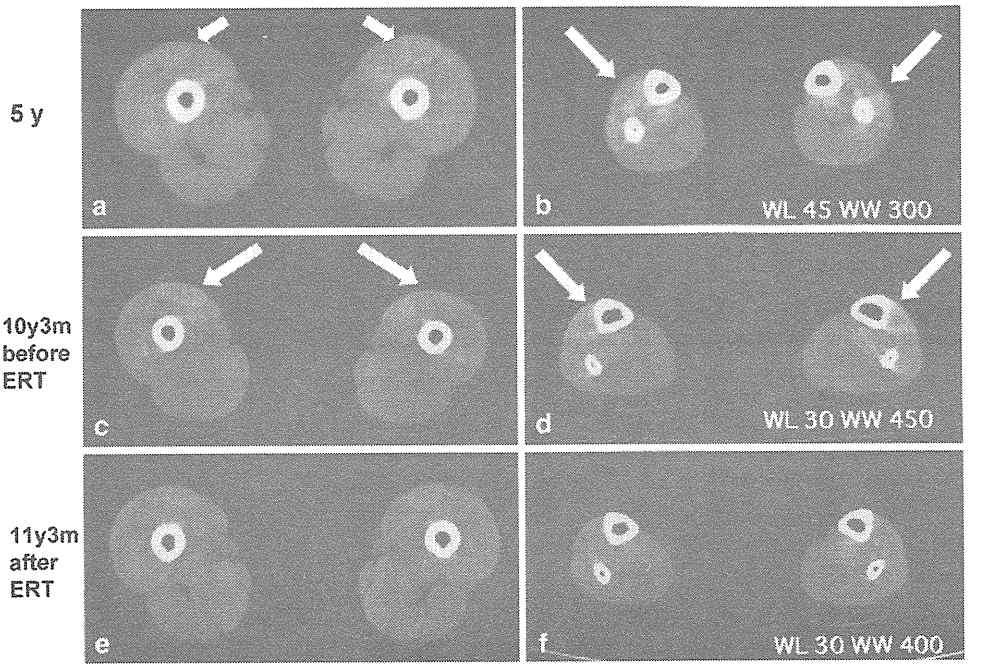

Fig. 2 Skeletal muscle CT scans in patient 2 at 5 years (**a**, **b**), 10 years (before ERT) (**c**, **d**) and 11 years (1 year after starting ERT) (**e**, **f**) of age. The rectus femoris (*arrows*) is only mildly affected, with no high-density areas (**a**), while the tibialis anterior (*arrows*) and peroneal muscles are more significantly involved and show high-density areas at age 5 years (**b**). Note evident high-density areas (*arrows*) in the rectus femoris at age 10 years (**c**). The high-density areas on CT were slightly reduced together with clinical improvement after ERT (**e**, **f**)

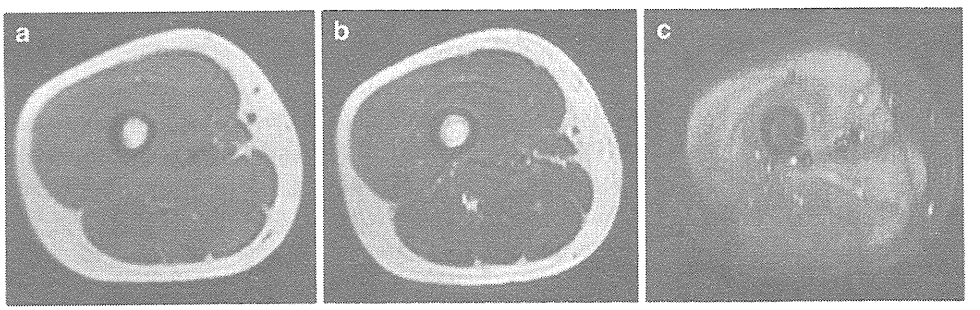

Fig. 3 Skeletal muscle MR images in patient 2 at 10 years of age. Very mildly increased intensity was recognized in the rectus femoris and adductor magnus on T1-weighted image (**a**). There was no detectable marked change on T2-weighted image (**b**). The high intensity was most clearly demonstrated in fat suppression on T1-weighted image (**c**)

4 months of this treatment, but they had returned to the original levels of 136/77 HU at 8 months and 140/80 at 1 year after starting ERT (Fig. 2e, f).

For comparison, we examined muscle MRI in patient 2 at 10 years of age (Fig. 3). Very mildly increased intensity was recognized in the rectus femoris and adductor magnus on T1-weighted images (Fig. 3a). The high intensity was more clearly demonstrated on fat suppression T1-weighted MRI (Fig. 3c) similar to that on CT. There was no marked change on T2-weighted images (Fig. 3b).

Morphological analysis

As we reported previously [1], histopathological findings were consistent with CT findings, i.e., the rectus femoris with extremely high-density areas on CT had numerous vacuoles filled with large amounts of glycogen (Fig. 5b), while the vastus lateralis muscles with normal CT density had a nearly normal appearance with few vacuoles (Fig. 5c) [1].

X-ray microanalysis with energy-dispersive X-ray spectroscopy (EDX) is an analytical technique used for elemental analysis of samples. In our patients' muscles, a mildly elevated Ca signal was detected in an area with glycogen accumulation (Fig. 4a, b), especially in electron dense globular bodies in vacuoles (Fig. 4c, d). As to disease controls, a low Ca signal was demonstrated in a few areas in a case with Duchenne muscular dystrophy, but none in muscles affected by dermatomyositis.

To demonstrate Ca deposition histochemically, we stained muscle biopsy specimens by the GBHA method in which insoluble red precipitates of Ca-GBHA complexes form under conditions of high Ca deposition. Nearly all of the fibers with vacuoles, in the specimens from the high-density areas on CT, were strongly reactive for GBHA (Fig. 5d),

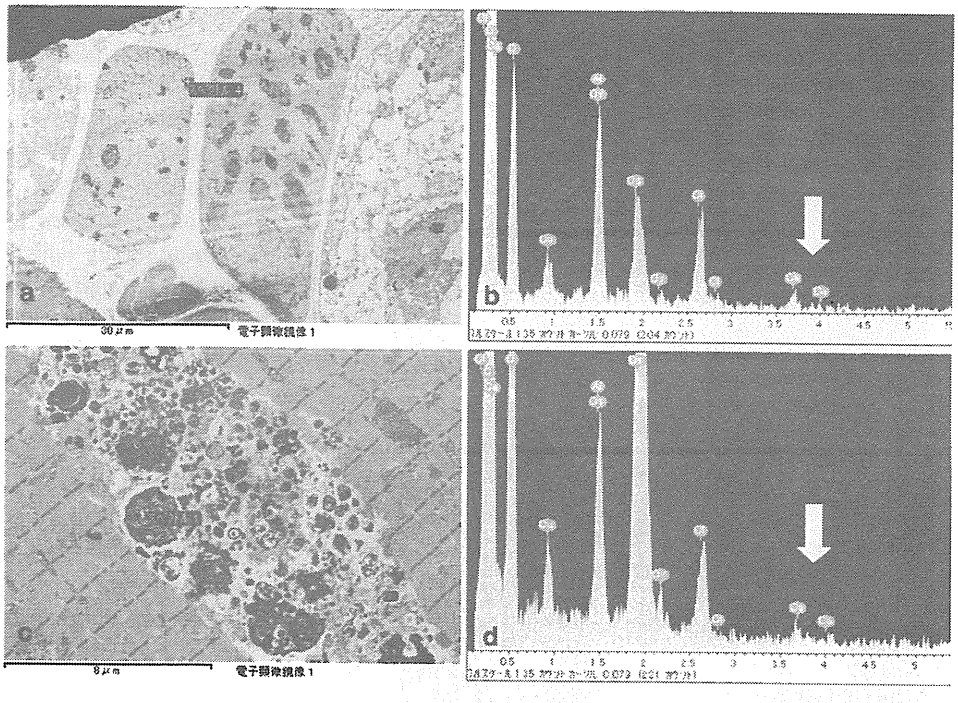

Fig. 4 X-ray microanalysis at 15 kV on an area (*arrow*) of excess glycogen accumulation (**a**) showed high Ca signals (**b**). At the electron dense globular bodies (*arrow*) (**c**), Ca signals were significantly elevated (**d**). **a**, **b** Electron micrographs from patient 2

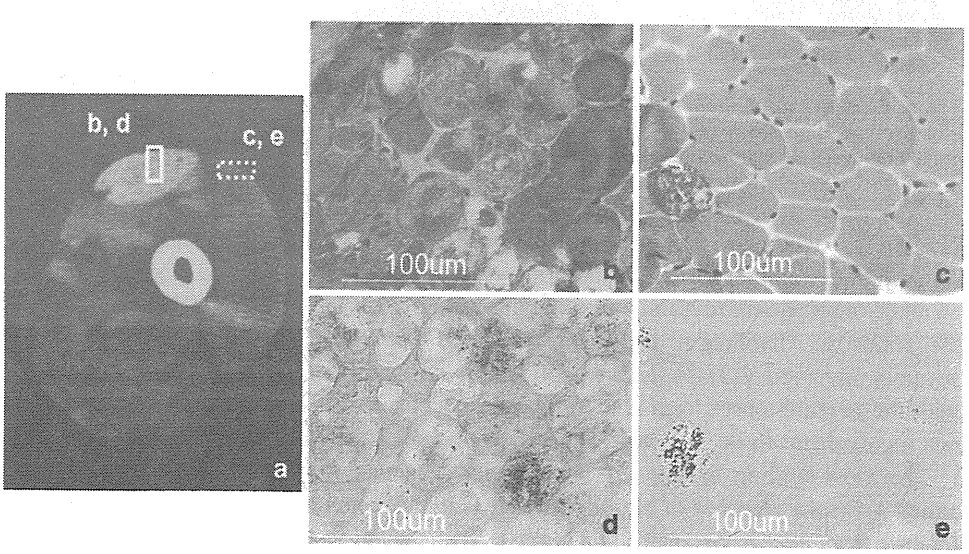

Fig. 5 Ca accumulation in rectus femoris muscles with high-density (*marked by solid line*) areas (**b**, **d**) and the vastus lateralis with normal CT density (*marked by dashed line*) (**c**, **e**) in the skeletal muscle CT scan (**a**) in patient 1 at 13 years of age. Numerous vacuoles filled with dense granular material (**b**) are strongly stained with GBHA (**d**) indicating increased amounts of Ca in the dense bodies. Note a few vacuolated fibers with calcium deposition in the less affected vastus lateralis muscle (**c**, **d**). **b**, **c** Hematoxylin and eosin staining, **d**, **e** GBHA staining

while GBHA reactions were localized in only a few affected fibers in muscles with normal density (Fig. 5e). GBHA positivity was not prominent in our two patients with the infantile-onset form or the two with the adult-onset form of Pompe disease. When we applied PAS staining to epon-embedded sections, dense globular bodies were strikingly prominent in the childhood form (Fig. 6a) but in neither the infantile- (Fig. 6b) nor the adult-onset form.

Discussion

In late-onset Pompe disease, including the childhood- and adult-onset forms, the most common feature is skeletal and respiratory muscle involvement sparing cardiac muscle. Whether the distribution-affected muscle differs between the two late-onset forms remains an open question. As observed in our patients, the anterior compartment of thigh muscles is preferentially involved in the childhood-onset form, and posterior thigh and truncal muscles in the adult-onset form [4, 5]. The affected muscles in the adult-onset form are atrophic with a moth-eaten, washed-out appearance. One report emphasized truncal muscle involvement mimicking that of facioscapulohumeral dystrophy [10].

Muscle MRI done on 11 patients with the adult-onset form [11] also demonstrated the posterior compartment of the thigh, including the adductor magnus and semimembranous muscles, to be affected from the early stage

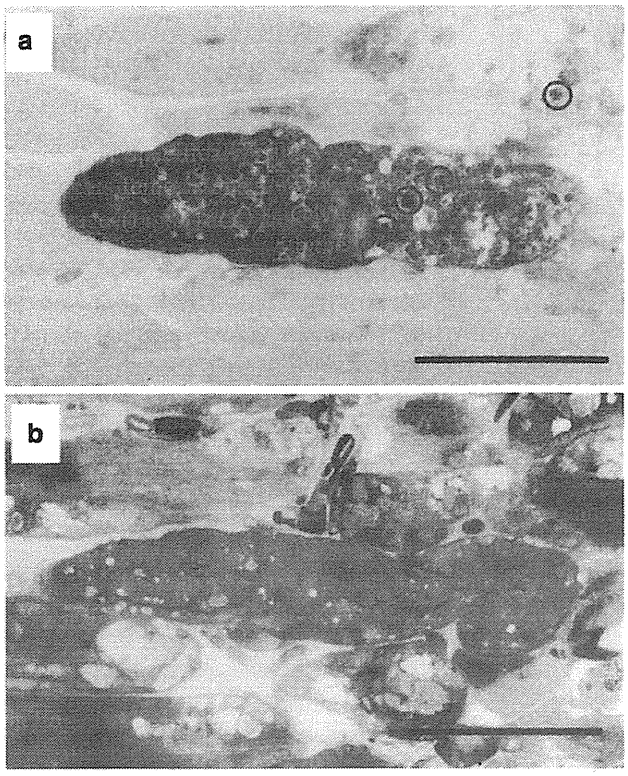

Fig. 6 Epon-embedded sections stained with PAS. Note that dense globular bodies (*circled*) in lysosomes are more prominent in the childhood-onset (**a**) than in infantile-onset (**b**) form. *Bar* 100 μm

ultimately extending to the long head of the biceps femoris, semitendinous and then anterior thigh muscles. Autopsy of an adult-onset patient revealed proximal muscles, including the iliopsoas, diaphragm and intercostals, to be most severely involved [13]. A recent MRI study on siblings with the juvenile-onset form also indicated adductor magnus involvement to be the earliest manifestation [6].

The most striking muscle CT abnormality seen in our patients was the presence of high-density areas in the rectus femoris from the early stage of this disease. These changes became increasingly prominent with age. High-density areas on CT scans have already been recognized as being consistent with the severity of pathological change, but the cause of these high-density changes remains uncertain. In patient 1, the high-density areas persisted into the third decade. Such high-density areas have not previously been documented in other myopathic disorders, including inflammatory myopathies and muscular dystrophies. Increased CT density has been described in glycogen-laden organs in various glycogen storage disorders including von Gierke's disease [2, 7, 8]. Glycogen solution reportedly exhibits an attenuation coefficient increase of 2.5–3.0 HU with each 1% increase in glycogen concentration in vitro [8]. Thus, excess glycogen itself can explain the increased CT density in patients with glycogen storage disorders.

Since the CT density in our patients was too high to simply reflect increased amounts of glycogen, we speculated that there were additional factors related to autophagic vacuoles, especially the end-products of autophagocytosis. It is well known that bleeding and calcification increase CT density. Therefore, we conducted X-ray microanalyses to identify the elements responsible for the observed density increases. This technique allows identification and assay of elements contained in samples by analyzing element-specific X-rays. Employing this method, we found high Ca signals in muscle specimens, especially in electron dense globular bodies in autophagic vacuoles. The strong GBHA staining also supports the concept of excess Ca accumulation in autophagic vacuoles. Therefore, Ca accumulation in autophagic vacuoles, rather than glycogen, appears to be the source of high-density areas in skeletal muscle on CT in childhood-onset Pompe disease patients. The mildly elevated intensity on T1-weighted images which was more clear on fat suppression on T1-weighted skeletal muscle MRI also supports calcification, rather than fatty replacement as in the adult-onset form. As shown in this patient, the muscle CT is much more informative than MRI for some disorders, especially chronic myopathies with calcification.

In muscular dystrophies, the hypercontracted fibers sometimes show high calcium accumulation. Since calcium in such fibers is soluble, the staining pattern is rather uniform which is quite different from granular pattern seen in the present biopsies. In other autophagic myopathies with rimmed vacuole formation and Danon disease, calcium accumulation was not found on GBHA staining (personal observation by Dr Nonaka).

Calcium accumulation in dense globular bodies in the lysosomes was confirmed by X-ray microanalysis and GBHA staining; however, its mechanism is not fully understood. Those dense bodies were not prominent in the infantile- and adult-onset forms. Since it may take some time to form dense globular bodies, probably via chronic degeneration of undigested glycogen particles in lysosomes, muscle degeneration may be too rapid to form such inclusion bodies with Ca accumulation in the infantile form. In the adult form, glycogen accumulation in the lysosomes and vacuolar formation are limited; therefore, calcium accumulation is not prominent. It is therefore quite reasonable that these high-density CT areas on CT are prominently seen in the childhood form, but not in other forms of Pompe disease.

Our findings came from only two patients, still we know that there are other Japanese patients with childhood-onset Pompe disease who show the exact same results such as high-density areas on skeletal muscle CT (personal communications). Study of a larger cohort will be helpful to confirm our hypothesis.

Acknowledgments This study was supported by the Research Grant (21B-12) for Nervous and Mental Disorders from the Ministry of Health, Labour and Welfare. The authors thank Drs. Hideo Sugie and Tokiko Fukuda, Jichi Children's Medical Center Tochigi, Jichi Medical University, for the biochemical analysis, Dr. Hiroshi Kobayashi, The Jikei University School of Medicine, Drs. Torayuki Okuyama and Eri Oda, National Center for Child Health and Development for the genetic analysis and Rieko Takahashi for technical assistance. We also thank Dr. Kayoko Saito, Institute of Medical Genetics, Tokyo Women's Medical University and Dr. Mitsuru Kawai, Higashi-Saitama National Hospital for clinical advice.

References

1. Arai Y, Osawa M, Shishikura K et al (1993) Computed tomography and magnetic resonance imaging of affected muscle in childhood acid alpha-glucosidase deficiency. Brain Dev 15:147–152
2. Biondetti PR, Fiore D, Muzzio PC (1980) Computed tomography of the liver in von Gierke's disease. J Comput Assist Tomogr 5:685–686
3. Calò M, Crisi G, Martinelli C, Colombo A, Schoenhuber R, Gibertoni M (1986) CT and the diagnosis of myopathies-preliminary findings in 42 cases. Neuroradiology 28:53–57
4. Cinnamon J, Slonim AE, Black KS, Gorey MT, Scuderi DM, Hyman RA (1991) Evaluation of the lumbar spine in patients with glycogen storage disease: CT demonstration of patterns of paraspinal muscle atrophy. Am J Neuroradiol 12:1099–1103
5. de Jager AEJ, van der Vilet TM, van der Ree TC, Oosterink J, Loonen MCB (1998) Muscle computed tomography in adult-onset acid maltase deficiency. Muscle Nerve 21:398–400
6. Dlamini N, Jan W, Norwood F et al (2008) Muscle MRI findings in siblings with juvenile-onset acid maltase deficiency (Pompe disease). Neuromuscul Disord 18:408–409
7. Doppman JL, Cornblath M, Dwyer AJ, Adams AJ, Girton ME, Sidbury J (1982) Computed tomography of the liver and kidneys in glycogen storage disease. J Comput Assist Tomogr 6:67–71
8. Dweyer A, Doppman JL, Adams AJ, Girton ME, Chernick SS, Cornblath M (1983) Influence of glycogen on liver density: computed tomography from a metabolic perspective. J Comput Assist Tomogr 7:70–73
9. Engel AG, Hirschhorn R, Huie ML (2004) Acid maltase deficiency. In: Engel AG, Franzini-Armstrong C (eds) Myology, vol 2, 3rd edn. McGraw Hill, New York, pp 1559–1580
10. Ohya Y, Morita H, Ogawa M, Nonaka I, Tsujino S, Kawai M (2001) A case of adult-onset acid maltase deficiency with affected muscles patterns resembling FSHD. Rinsho-Shinkei 41:390–396 (in Japanese)
11. Pichiecchio A, Uggetti C, Ravaglia S et al (2004) Muscle MRI in adult-onset acid maltase deficiency. Neuromuscul Disord 14:51–55
12. Swash M, Brown MM, Thakkar C (1995) CT muscle imaging and the clinical assessment of neuromuscular disease. Muscle Nerve 18:708–714
13. Van der Walt JD, Swash M, Leake J, Cox EL (1987) The pattern of involvement of adult-onset acid maltase deficiency at autopsy. Muscle Nerve 10:272–281
14. Vliet AM, Thijssen HOM, Joosten E, Merx JL (1988) CT in neuromuscular disorders: a comparison of CT and histology. Neuroradiology 30:421–425

JPSA
Japan Poultry Science Association

http://www.jstage.jst.go.jp/browse/jpsa
doi:10.2141/jpsa.46.95

Expression Pattern of *WWP1* in Muscular Dystrophic and Normal Chickens

Hirokazu Matsumoto[1], Hideaki Maruse[1], Shinji Sasazaki[1], Akira Fujiwara[2], Shin'ichi Takeda[3], Nobutsune Ichihara[4,5], Tateki Kikuchi[3], Fumio Mukai[1] and Hideyuki Mannen[1]

[1] Laboratory of Animal Breeding and Genetics, Graduate School of Agricultural Science, Kobe University, Kobe 657-8501, Japan
[2] Laboratory Animal Research Station, Nippon Institute for Biological Science, Kobuchisawa 408-0041, Japan
[3] Department of Molecular Therapy and of [4] Animal Models for Human Disease, National Institute of Neuroscience, NCNP, Kodaira, Tokyo 182-8502, Japan
[5] Department of Anatomy I, School of veterinary medicine, Azabu University, Fuchinobe, Sagamihara, Kanagawa 229-8501, Japan

The WW domain containing E3 ubiquitin protein ligase 1 (WWP1) is classified into one of ubiquitin ligases which play an important role in ubiquitin-proteasome pathway. Previously, we identified the *WWP1* gene as a candidate gene of chicken muscular dystrophy by linkage analysis and sequence comparison. However, the mechanism causing pathological changes and underlaying gene function remains elucidated. In the present study, we analyzed the *WWP1* gene expression in various muscles and tissues of normal chickens, and compared with those from muscular dystrophic chickens. Two mRNA isoforms were detected in all tissues examined and revealed almost equal expression level. The *WWP1* expression of dystrophic chickens was decreased in almost all skeletal muscles including unaffected muscles. These data indicate that there might not be a causal relationship between the alteration of *WWP1* expression level and the severity of muscular dystrophy.

Key words: chicken, expression analysis, fast twitch muscle fiber, muscular dystrophy, WWP1

J. Poult. Sci., 46: 95-99, 2009

Introduction

The WW domain containing E3 ubiquitin protein ligase 1 (*WWP1*) is classified into an ubiquitin ligase (E3) which plays an important role in ubiquitin-proteasome pathway (UPP) to degrade unneeded or damaged proteins (Scheffner and Staub, 2007). E3 recognizes and catalyzes ubiquitin (Ub) conjugation to specific protein substrates (Liu, 2004). Comparative genome analysis reveals few genes encoding E1, tens of E2 encoding genes and hundreds of E3 encoding genes (Semple *et al.*, 2003).

The *WWP1* gene is classified into HECT (homologous to the E6-AP carboxyl terminus)-type E3 which possesses one C2 domain, multiple WW domains and one HECT domain (Pirozzi *et al.*, 1997; Flasza *et al.*, 2002). The C 2 domain binds to the cellular membranes in a Ca^{2+}-dependent manner (Plant *et al.*, 1997) and mediates interactions with other proteins (Plant *et al.*, 2000; von Poser *et al.*, 2000; Augustine, 2001). The WW domain has two conserved tryptophan residues and binds proline-rich region (Sudol *et al.*, 1985). HECT domain, similar to E2s structurally, has a cysteine residue as an active center that transfers the activated Ub from E2 onto first itself, and then onto its substrates (Jackson *et al.*, 2000).

The muscular dystrophies are the group of inherited diseases with progressive weakness and degeneration of skeletal muscle (Partridge, 1991). It is well known that abnormalities of muscle proteins linking sarcolemma and basal lamina lead to cause muscular dystrophies (Lisi and Cohn, 2007), but there are a number of muscular dystrophies and related diseases of which causes are still unknown. We identified *WWP1* gene as a candidate responsible for the chicken muscular dystrophy by the linkage analysis (Matsumoto *et al.*, 2007) and the sequence comparison between normal and dystrophic chickens (Matsumoto *et al.*, 2008). The R441Q missense mutation was found in *WWP1* gene to cause the phenotype of muscular dystrophy.

The WWP1s of human (Flasza *et al.*, 2002; Komuro *et al.*, 2004), mouse (Dallas *et al.*, 2006) and *C. elegans* (Huang *et al.*, 2000) were intensively studied and known

Received: October 10, 2008, Accepted: December 24, 2008
Correspondence: Dr. H. Mannen, Graduate School of Agricultural Science, Kobe University, Kobe 657-8501, Japan.
(E-mail: mannen@kobe-u.ac.jp)

that the *WWP1* gene is expressed ubiquitously, but strongly in liver, bone marrow, testis and skeletal muscles (Flasza *et al.*, 2002; Komuro *et al.*, 2004). In chicken, however, the *WWP1* expression has not been studied. The expression analysis of *WWP1* gene is important since it was reported that altered expression of known responsible gene could lead dystrophic phenotype (Smythe and Rando, 2006).

In this study, we analyzed the mRNA expression of *WWP1* in various skeletal muscles and other tissues of normal and dystrophic chickens by using Northern blotting and reverse transcription (RT)-PCR analysis to know the differences in the general expression pattern between them.

Materials and Methods

Chickens

A two-month-old dystrophic chicken (New Hampshire: NH-413) and an age-matched normal chicken (White Leghorn: WL-F) were used in this study. The New Hampshire (NH-413) strain is a homozygous dystrophic line introduced from University of California, Davis to Japan in 1976 (Kondo *et al.*, 1982). The disease in this strain is transmitted co-dominantly by a single gene, but the phenotype is modified by other background genes (Kikuchi *et al.*, 1981, 1987; Wilson *et al.*, 1979). The White Leghorn (WL-F) strain was established in 1970s, and maintained as closed colony in the Nippon Institute of Biological Science in Yamanashi, Japan. This study was carried out according to the guidelines of Animal Experimentation of Kobe University.

Expression analysis

For Northern blotting, mRNAs were isolated from *M. pectoralis superficialis* (PS), *M. tensor fascia lata* (TFL), *M. biceps femoris* (BF), *M. triceps surae* (TS), *M. peroneus longus* (PL), heart (H), brain (B), liver (L), kidney (K) and whole embryo (E) with PolyATtract mRNA Isolation kit (Promega, Madison, WI, USA). The 2μg of mRNAs, which were measured with NanoDrop ND-1000 spectrophotometer (NanoDrop Technologies, Wilmington, DE, USA), were resolved by 1.2% agarose gel electrophoresis in the presence of formaldehyde and blotted on to Hybond-N+membrane (GE Healthcare Bio-Sciences AB, Uppsala, Sweden). The mRNAs were visualized using digoxigenin (DIG) reagents, and kits for non-radioactive nucleic acid labeling and detection system (Roche Diagnostics, Basel, Switzerland) according to the procedure specified by the manufacturer excepting that the washing was done with 4×SCC 0.1% SDS at room temperature for 10 min, 4×SCC 0.1% SDS at 40℃ for 8 min and then 2×SCC 0.1% SDS at 40℃ for 8 min twice. The DIG-labeled DNA probes were prepared by PCR using DIG-dUTP using pectorals cDNA sample of a WL-F strain female as a template. The primers applied in this procedure were 5′-tccctcataaatgttgaaagcagaca-3′ (WWP1p-F), 5′-gtaataacccaaggtaatatgtaaac-3′ (WWP1 p-R) (NM_001012554), 5′-ccgtgtgccaacccccaatgt ctctg-3′ (GAPDHp-F) and 5′ -cagtttctatcagcctctcccacctc- 3′ (GAPDHp-R) (NM_204305). The PCR was done for 35 cycles at 94℃ for 30 sec, 55℃ for 30 sec, 72℃ for 30 sec (*WWP1*) and for 35 cycles at 94℃ for 30 sec, 63℃ for 30 sec, 72℃ for 30 sec (*GAPDH*) using TaKaRa Ex Taq® Hot Start Version (Takara Bio Inc., Tokyo, Japan). Quantitative analysis was performed with Scion Image (Scion Corporation, Frederick, MD, USA).

In order to analyze mRNA expression of *WWP1* gene in the PS, *M. anterior latissimus dorsi* (ALD) and H, RT-PCR method was applied. The concentration of cDNA derived from these muscles was calculated by NanoDrop ND-1000 (NanoDrop Technologies) and commeasurable cDNAs were used as template. The primers applied were 5′-attaggaagagccactgtagact-3′ (WWP1r-F) and 5′-tctgttgattgaggttctgctgt-3′ (WWP1r-R) (NM_001012554). The PCR was done for 35 and 40 cycles at 94℃ for 30 sec, 56℃ for 30 sec, 72℃ for 30 sec using TaKaRa Ex Taq® Hot Start Version (Takara Bio Inc.).

Histology

The PS, ALD and H were snap-frozen in liquid nitrogen-cooled isopentane and sectioned in a cryostat (Leica Microsystems Japan, Tokyo, Japan). The histopathology was made by hematoxylin-eosin staining (HE) method (Kikuchi *et al.*, 1981).

Results

The mRNA expression of *WWP1* gene was detected by Northern blotting in various muscles and other tissues of normal and muscular dystrophic chickens (Fig. 1). Two bands were detected in all tissues examined, and revealed almost equally expression level in any muscles and tissues observed.

In the PS, BF, TS, PL, B and K, *WWP1* gene was strongly expressed in normal than in dystrophic chickens (Fig. 1). *GAPDH* was used as an internal control of *WWP 1* expression analysis. In TFL, L and E, similar *WWP1* expression level was observed between two phenotypes (Fig. 1).

RT-PCR analysis indicated that *WWP1* gene was expressed in slow tonic ALD, not only in PS and H of both phenotypes (Fig. 2A). Figure 2B shows histopathological changes in PS, ALD and H of normal and dystrophic chickens. The pathological findings in dystrophic PS were characterized by the degenerating fibers with many vacuoles in cytoplasm, the fatty infiltration into connective tissue, and the proliferation of nuclei within muscle fibers with large variation in sizes. However, no such lesions were observed in ALD and H from age-matched dystrophic chickens (Fig. 2B).

Discussion

Northern blotting with *WWP1* specific probe detected two bands in all tissues and muscles examined (Fig. 1). Northern blot analysis of *WWP1* expression in human tissues also exhibited two bands (Mosser *et al.*, 1998), and RT-PCR analysis showed that human *WWP1* gene had at

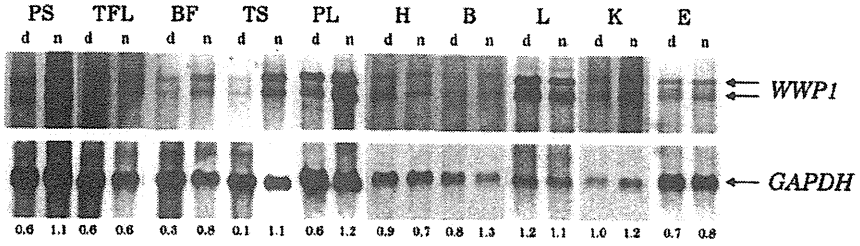

Fig. 1. **Expression of chicken *WWP1* in various tissues.**
A *WWP1* cDNA probe was used to detect *WWP1* mRNA transcripts by Northern blotting using blots containing 2μg of mRNAs from chicken muscles or various other tissues. *M. pectoralis superficialis* (PS), *M. tensor fascia lata* (TFL), *M. biceps femoris* (BF), *M. triceps surae* (TS), *M. peroneus longus* (PL), heart (H), brain (B), liver (L), kidney (K) and embryo (E) were analyzed. A doublet band is detected at variable levels in all tissues. "d" indicates mRNAs from dystrophic chickens. "n" indicates mRNAs from normal chickens. The numbers below the *GAPDH* bands represent the relative ratios of *WWP1/GAPDH*.

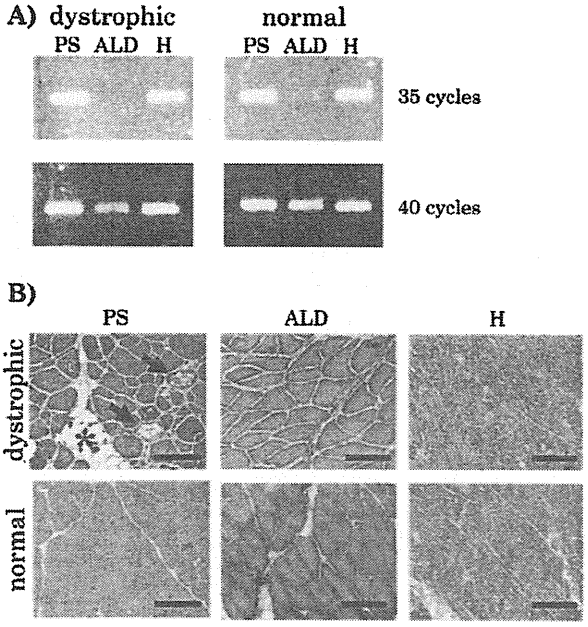

Fig. 2. **RT-PCR detection of *WWP1* gene and histological analysis for three representative muscle types.**
M. pectoralis superficialis (PS), *M. anterior latissimus dorsi* (ALD) and heart (H) expressed *WWP1* less in muscular dystrophic chicken, but only dystrophic PS was severely harmed. A) Expression of *WWP1* in PS, ALD and H was analyzed by RT-PCR method. PCR was performed for 35 or 40 cycles. B) The PS, ALD and H of dystrophic (NH-413) and normal (WL-F) chickens were analyzed with HE staining. Vacuoles (arrows) and fatty infiltration (asterisk) are observed in PS of dystrophic chickens. It is also remarkable that, in dystrophic PS, many muscle fibers have many nuclei in cytoplasm and vary widely in size. These pathological features are not observed in ALD and H of dystrophic chicken. Scale bar = 120μm.

least six mRNA isoforms synthesized through the alternative splicing, two of which were strongly expressed and commonly observed in various tissues (Flasza *et al.*, 2002). The mRNA doublet bands of chicken *WWP1* by Northern blot analysis might be equivalent to two bands of human tissues, while a single band was observed by RT-PCR analysis in chicken (Fig. 2A), suggesting that the amplified region does not include alternative spliced site. Flasza *et al.* (2002) also mentioned that the relative ratio of these isoforms from human *WWP1* varied in a tissue-specific manner, but the doublet bands of chicken *WWP1* were expressed almost equally in all tissues examined.

The *WWP1* gene expression in *M. pectoralis superficialis* (PS) of dystrophic chicken was less than that of normal chicken (Fig. 1). The PS of chicken is a fast twitch muscle composed of two types of fast twitch fibers (αW and βW). TFL, BF, TS and PL muscles from wing and leg are mixed muscles co-existing fast twitch (αW and βW) with slow twitch fibers (βR) in a mosaic pattern (Ashmore and Doerr, 1971a), except that the ALD and *M. adductor magnus* are composed of slow tonic fibers (ST) innervated multiply (Ashmore *et al.*, 1978; Kikuchi *et al.*, 1986). In chicken muscular dystrophy, fast twitch fibers are initially and most severely affected, while slow twitch and slow tonic muscles persist relatively harmless throughout the life span (Ashmore and Doerr, 1971b; Barnard *et al.*, 1982). The *WWP1* expression in dystrophic BF, TS and PL showed a similar downward trend as observed in dystrophic PS (Fig. 1). These data indicate that there might not be a causal relationship between the alteration of *WWP1* expression level and the severity of muscular dystrophy, since not only affected muscles but unaffected ones exhibited the same pattern. Moreover, the alteration of *WWP1* expression level was observed in other unaffected tissues, such as B and K, which reinforces our hypothesis that the alteration of *WWP1* expression levels

does not link directly to the dystrophic phenotype (Fig. 1).

To assess the genetic influence of mutant *WWP1* upon chicken muscular dystrophy, we examined *WWP1* gene expression and histological changes in three distinct muscle types, PS as a fast twitch type, ALD as a slow tonic type, and H as a different type of muscle. RT-PCR was applied to this study since ALD was not enough quantity of mRNA for Northern blotting. The *WWP1* mRNA expression was confirmed in all muscles examined (Fig. 2 A).

Figure 2B shows HE stained sections of PS, ALD and H from normal and dystrophic chicken. The dystrophic PS was severely affected, while ALD and heart of dystrophic chicken remained relatively intact (Fig. 2B) as described in a previous study (Kikuchi *et al.*, 1981). The *WWP1* was expressed even in unaffected muscles and the downward alteration of *WWP1* expression was observed commonly in almost all dystrophic muscles examined (Figs. 1, 2). The observation suggests that the alteration of *WWP1* might not be the cause of the pathological change in chicken muscular dystrophy. Hence, the mutation identified previously (Matsumoto *et al.*, 2008) might play a crucial role in leading the onset of chicken muscular dystrophy. The detected mutation lay between WW domains, highly conserved region among tetrapods (Matsumoto *et al.*, 2008), which has been predicted as substrate binding region (Pirozzi *et al.*, 1997; Flasza *et al.*, 2002). This suggests that mutated *WWP1* could not recognize its substrates.

Many HECT-type E3s with WW domains including *WWP1* regulate membrane proteins (Chen and Matesic, 2007). Therefore, aberrant regulation of membrane protein may lead the onset of chicken muscular dystrophy. For example, *WWP1* could bind to β-dystroglycan, which is one of important muscle proteins consisting of membrane (Pirozzi *et al.*, 1997). Abnormal glycosylation of α-dystroglycan in chicken muscular dystrophy has been reported (Saito *et al.*, 2005). Furthermore, the fact that some E3s can recognize sugar chain (Yoshida *et al.*, 2002, 2003; Lederkremer and Gliskman, 2005) leads to the hypothesis that mutated *WWP1* might not be able to recognize the sugar chain of α-dystroglycan to regulate the glycosylated molecules, and that insufficiently glycosylated α-dystroglycan accumulates and causes the disease.

In the present study, we analyzed the mRNA expression of *WWP1* in various skeletal muscles and other tissues of normal and dystrophic chickens. The results suggest that *WWP1* expression level lowered in dystrophic phenotype is not directly related to the cause of disease in chicken muscular dystrophy, whereas mutated *WWP1* does not function normally to cause the onset of chicken muscular dystrophy.

Acknowledgments

This work was supported in part by Grant-in-Aid for Scientific Research (C), no. 19580338, and the Global COE Program "Global Center for Education and Research in Integrative Membrane Biology" (A-8) from the Ministry of Education, Science, Sports and Research on Nervous and Mental Disorders (16B-2, 19A-7) from the Japanese Ministry of Health, Labor and Welfare.

References

Ashmore CR and Doerr L. Comparative aspects of muscle fiber types in different species. Experimental Neurology, 31: 408–418. 1971a.

Ashmore CR and Doerr L. Postnatal development of fiber types in normal and dystrophic skeletal muscle of the chick. Experimental Neurology, 30: 431–446. 1971b.

Ashmore CR, Kikuchi T and Doerr L. Some observations on the innervation patterns of different fiber types of chick muscle. Experimental Neurology, 58: 272–284. 1978.

Augustine GJ. How does calcium trigger neurotransmitter release? Current Opinion in Neurobiology, 11: 320–326. 2001.

Barnard EA, Lyles JM, and Pizzey JA. Fibre types in chicken skeletal muscles and their changes in muscular dystrophy. The Journal of Physiology, 331: 333–354. 1982.

Chen C and Matesic LE. The Nedd4-like family of E3 ubiquitin ligases and cancer. Cancer Metastasis Reviews, 3–4: 587–604. 2007.

Dallas CJ, Marc NW, Mohamed O, Jochen GH, Melvin JG and Laurie HG. Regulation of Adult Bone Mass by the Zinc Finger Adapter Protein Schnurri-3. Science, 312: 1223–1227. 2006.

Flasza M, Gorman P, Roylance R, Canfield AE and Baron M. Alternative Splicing Determines the Domain Structure of WWP1, a Nedd4 Family Protein. Biochemical and Biophysical Research Communications, 290: 431–437. 2002.

Huang K, Johnson KD, Petcherski AG, Vandergon T, Mosser EA, Copeland NG, Jenkins NA, Kimble J and Bresnick EH. A HECT domain ubiquitin ligase closely related to the mammalian protein WWP1 is essential for Caenorhabditis elegans embryogenesis. Gene, 252: 137–145. 2000.

Jackson PK, Eldridge AG, Freed E, Furstenthal L, Hsu JY, Kaiser BK and Reimann JDR. The lore of the RINGs: substrate recognition and catalysis by ubiquitin ligases. Trends in Cell Biology, 10: 429–439. 2000.

Kikuchi T, Ishiura S, Nonaka I and Ebashi S. Genetic heterozygous carriers in hereditary muscular dystrophy of chickens. Tohoku Journal of Agriculture Research, 32: 14–26. 1981.

Kikuchi T, Akiba T and Ashmore CR. Conversion of muscle fiber types in regenerating chicken muscles following cross-reinnervation. Acta Neuropathologica, 71: 197–206. 1986.

Kikuchi T, Moriya H, Matuzani T, Katoh M and Takeda S. The development of laboratory animal science for the study of human muscular and nervous diseases in Japan. Congenital Anomalies, 27: 447–462. 1987.

Komuro A, Imamura T, Saitoh M, Yoshida Y, Yamori T, Miyazono K and Miyazawa K. Negative regulation of transforming growth factor-beta (TGF-beta) signaling by WW domain-containing protein 1 (WWP1). Oncogene, 23: 6914–6923. 2004.

Kondo K, Kikuchi T and Mizutani M. Breeding of the chicken as an animal model for muscular dystrophy. In: Muscular Dystrophy (Ebashi S ed.), pp. 19–24. Tokyo University

Press. Tokyo. 1982.
Lederkremer GZ and Glickman MH. A window of opportunity: timing protein degradation by trimming of sugars and ubiquitins. Trends in Biochemical Sciences, 30: 297-303. 2005.
Lisi MT and Cohn RD. Congenital muscular dystrophies: new aspects of an expanding group of disorders. Biochimica et Biophysica Acta, 1772: 159-172. 2007.
Liu YC. Ubiquitin ligases and the immune response. Annual Review of Immunology, 22: 81-127. 2004.
Matsumoto H, Maruse H, Yoshizawa K, Sasazaki S, Fujiwara A, Kikuchi T, Ichihara N, Mukai F and Mannen H. Pinpointing the candidate region for muscular dystrophy in chickens with an abnormal muscle gene. Animal Science Journal, 78: 476-483. 2007.
Matsumoto H, Maruse H, Inaba Y, Yoshizawa K, Sasazaki S, Fujiwara A, Nishibori M, Nakamura A, Takeda S, Ichihara N, Kikuchi T, Mukai F and Mannen H. The ubiquitin ligase gene (WWP1) is responsible for the chicken muscular dystrophy. FEBS Letters, 582: 2212-2218. 2008.
Mosser EA, Kasanov JD, Forsberg EC, Kay BK, Ney PA and Bresnick EH. Physical and functional interactions between the transactivation domain of the hematopoietic transcription factor NF-E2 and WW domains. Biochemistry, 37: 13686-13695. 1998.
Partridge T. Animal models of muscular dystrophy: what can they teach us? Neuropathology and Applied Neurobiology, 17: 353-363. 1991.
Pirozzi G, McConnell SJ, Uveges AJ, Carter JM, Sparksi AB, Kayi BK and Fowlkes DM. Identification of Novel Human WW Domain-containing Proteins by Cloning of Ligand Targets. The Journal of Biological Chemistry, 272: 14611-14616. 1997.
Plant PJ, Lafont F, Lecat S, Verkade P, Simons K and Rotin D. Apical membrane targeting of Nedd4 is mediated by an association of its C2 domain with annexin XIIIb. The Journal of Cell Biology, 149: 1473-1484. 2000.
Plant PJ, Yeger H, Staub O, Howard P and Rotin D. The C2 domain of the ubiquitin protein ligase Nedd4 mediates Ca^{2+}-dependent plasma membrane localization. The Journal of Biological Chemistry, 272: 32329-32336. 1997.
Saito F, Blank M, Schroder J, Manya H, Shimizu T, Campbell KP, Endo T, Mizutani M, Kroger S and Matsumura K. Aberrant glycosylation of a-dystroglycan causes defective binding of laminin in the muscle of chicken muscular dystrophy. FEBS Letters, 579: 2359-2363. 2005.
Scheffner M and Staub O. HECT E3s and human disease. BMC Biochemistry, 8 Suppl 1: S6. 2007.
Semple CA, RIKEN GER Group and GSL Members. The comparative proteomics of ubiquitination in mouse. Genome Research, 13: 1389-1394. 2003.
Smythe GM and Rando TA. Altered caveolin-3 expression disrupts PI (3) kinase signaling leading to death of cultured muscle cells. Experimental cell research, 312: 2816-2825. 2006.
Sudol M, Chen HI, Bougeret C, Einbond A and Bork P. Characterization of a novel protein-binding module: the WW domain. FEBS Letters, 369: 67-71. 1985.
von Poser C, Zhang JZ, Mineo C, Ding W, Ying Y, Sudhof TC and Anderson RG. Synaptotagmin regulation of coated pit assembly. The Journal of Biological Chemistry, 275: 30916-30924. 2000.
Wilson BW, Randall WR, Patterson GT and Entrikin RK. Major physiologic and histochemical characteristics of inherited dystrophy of the chicken. Annals of the New York Academy of Sciences, 317: 224-246. 1979.
Yoshida Y, Chiba T, Tokunaga F, Kawasaki H, Iwai K, Suzuki T, Ito Y, Matsuoka K, Yoshida M, Tanaka K and Tai T. E 3 ubiquitin ligase that recognizes sugar chains. Nature, 418: 438-442. 2002.
Yoshida Y, Tokunaga F, Chiba T, Iwai K, Tanaka K and Tai T. Fbs2 is a new member of the E3 ubiquitin ligase family that recognizes sugar chains. The Journal of Biological Chemistry, 278: 43877-43884. 2003.

ABSTRACT: Duchenne muscular dystrophy (DMD) is a devastating muscle disorder that is characterized by progressive muscle necrosis, fibrosis, and fatty infiltration. To examine the temporospatial pathological changes, a noninvasive evaluation method such as magnetic resonance imaging (MRI) is needed. The aim of this study was to precisely assess muscle necrosis and inflammation based on a sequence of T2-weighted imaging (T2WI), gadolinium-enhanced imaging, and selective fat suppression, chemical shift selective T2-weighted imaging (CHESS-T2WI), on a 3.0-Tesla MRI unit in 3-month-old and 7-year-old dogs with canine X-linked muscular dystrophy ($CXMD_J$), a suitable animal model for DMD. The results show that CHESS-T2WI was more sensitive and useful from the early to late stages of $CXMD_J$ than T2WI or contrast enhancement imaging in the evaluation of muscle necrosis, because these latter sequences can be influenced by fatty infiltration or interstitial connective tissues.

Muscle Nerve **40:** 815–826, 2009

EVALUATION OF DYSTROPHIC DOG PATHOLOGY BY FAT-SUPPRESSED T2-WEIGHTED IMAGING

MASANORI KOBAYASHI, DVM,[1,2] AKINORI NAKAMURA, MD, PhD,[1] DAISUKE HASEGAWA, DVM, PhD,[2] MICHIO FUJITA, DVM, PhD,[2] HIROMITSU ORIMA, DVM, PhD,[2] and SHIN'ICHI TAKEDA, MD, PhD[1]

[1] Department of Molecular Therapy, National Institute of Neuroscience, NCNP, 4-1-1 Ogawa-higashi, Kodaira, Tokyo 187-8502, Japan
[2] Department of Veterinary Radiology, Nippon Veterinary and Life Science University, Tokyo, Japan

Accepted 23 March 2009

Duchenne muscular dystrophy (DMD) is a severe X-linked muscle disease characterized by progressive skeletal muscle atrophy and weakness.[1] DMD is caused by mutations in the *dystrophin* gene, which encodes the cytoskeletal protein dystrophin.[2] A loss of dystrophin accompanied by a deficiency of dystrophin–glycoprotein complex (DGC) from the sarcolemma leads to progressive degeneration of striated muscle.[3,4] In dystrophic skeletal muscles, muscle fiber necrosis with inflammation is followed by muscle regeneration, but the muscle is finally replaced by fibrous or fatty tissue.[5,6] For this devastating disorder, various therapeutic approaches, such as gene therapy, stem cell–based cell therapy, or pharmaceutical agents have been proposed and explored using various DMD animal models.

The X-linked muscular dystrophy (*mdx*) mouse and Golden Retriever muscular dystrophy (GRMD) dog are the most commonly used DMD animal models.[7,8] *mdx* mice show extensive necrosis followed by regeneration, but their phenotypes are milder than those of DMD due to the absence of apparent fibrosis and fatty infiltration.[7,9,10] The phenotypes of striated muscle in the GRMD dog are clinically and pathologically more similar to that of DMD,[8,11,12] but it is very difficult to maintain this animal model due to the severe phenotype. We have therefore established a Beagle-based colony of canine X-linked muscular dystrophy in Japan ($CXMD_J$).[13] We have found that the clinical and pathological findings in $CXMD_J$ are similar to but milder than those in GRMD.[14,15]

A method of noninvasive temporospatial assessment is required to investigate muscle involvement and, especially, to evaluate therapeutic

Abbreviations: ANOVA, analysis of variance; CE, contrast enhancement ratio; CHESS, chemical shift selective; CT, computed tomography; $CXMD_J$, canine X-linked muscular dystrophy in Japan; DGC, dystrophin–glycoprotein complex; DMD, Duchenne muscular dystrophy; EDL, extensor digitorum longus; FDS, flexor digitorum superficialis; FITC, fluorescein isothiocyanate; GC, gastrocnemius; Gd-DTPA, gadolinium diethylenetriamine pentaacetic acid; GMRD, Golden Retriever muscular dystrophy; MRI, magnetic resonance imaging; PCr, phosphocreatine; Pi, inorganic phosphate; ROI, region of interest; SNR, signal-to-noise ratio; STIR, short-tau inversion recovery; SI, signal intensity; TC, tibialis cranialis

Key words: chemical shift selective fat-suppressed T2-weighted imaging; Duchenne muscular dystrophy; dystrophic dog; magnetic resonance imaging; myopathy

Correspondence to: S. Takeda; e-mail: takeda@ncnp.go.jp

Published online 7 August 2009 in Wiley InterScience (www.interscience.wiley.com). DOI 10.1002/mus.21384

interventions. Computed tomography (CT), which shows high temporal and spatial resolution, has been used to detect selective muscle involvement, such as atrophy or fatty tissue replacement, in patients suffering from DMD,[16,17] but it requires ionizing radiation and has limited sensitivity for soft tissues.[18] Magnetic resonance imaging (MRI) produces high-resolution images with good contrast among soft tissues,[19] and therefore it has been used to evaluate skeletal muscle involvement in DMD[20] and in *mdx* mice.[21] In the early stages of dystrophy, the T1 relaxation time is prolonged due to muscle degeneration and regeneration together with an increase in muscle water concentration, and it is decreased owing to fat infiltration in the advanced stage.[22] As the main magnetic field increases, however, the capacity to differentiate tissues on the basis of T1 relaxation time may decrease.[23] On the other hand, the T2 relaxation time is prolonged in necrotic as well as fatty and connective tissue[19]; therefore, it can hardly distinguish necrosis from fat replacement or fibrosis during the dystrophic process. To selectively detect necrotic changes, MR contrast agents, such as gadolinium diethylenetriamine pentaacetic acid (Gd-DTPA), have been used extensively,[24–26] but these agents may also enhance blood vessels and the interstitium,[27] and may cause severe adverse effects, such as anaphylaxis,[28,29] which are critical for DMD patients. Thus, a safer imaging protocol is needed to distinguish necrotic lesions from fatty degeneration or fibrosis in the dystrophic skeletal muscle of DMD and $CXMD_J$.

To discriminate necrosis from fatty infiltration, one of the fat suppression sequences may be useful. As a fat suppression sequence, short-tau inversion recovery (STIR) MR imaging was used to detect muscle edema in DMD.[6] However, STIR suppresses the signal from any tissue or fluid that has a short T1 relaxation time, and therefore it does not selectively suppress the fat signal.[30,31] In contrast, chemical shift selective (CHESS) imaging, another fat suppression sequence, is a technique that selectively saturates fat magnetization by applying a 90° pulse matching with the fat resonance frequency and therefore leads to a highly selective suppression of fat signals. Moreover, the signal-to-noise ratio (SNR) of CHESS is better than that of STIR at a higher magnetic field. The sequence of CHESS combined with T2-weighted imaging (CHESS-T2WI) has been used to diagnose disorders such as lipomatous tumor or temporomandibular arthrosis.[32–34] The method, however, has not been applied to evaluation of the dystrophic changes seen in DMD or the animal models to date.

We, therefore, examined dystrophic dog muscle by CHESS-T2WI to determine whether this sequence is more useful for finding necrosis and inflammatory change than the conventional sequences of T2WI or contrast imaging.

METHODS

Animals. We used three 3-month-old normal male dogs (II-2308MN, II/III-3911MN, and II-4202MN), three littermate $CXMD_J$ male dogs (II-2302MA, II/III-3903MA, and II-4204MA), one 7-year-old normal male dog (00-174MN), and two 7-year-old $CXMD_J$ male dogs (II-C04MA and II-C12MA). II-2308MN, II-4202MN, II-2302MA, and II-4204MA were produced by mating a second-generation (G2) carrier female[13] and G2 affected male. II/III-3911MN and II/III-3903MA were the offspring of a G2 carrier female and a third-generation (G3) affected male. We obtained II-C04MA and II-C12MA by mating first-generation (G1) carrier female dogs and pure-bred normal male Beagles. 00-174MN was a pure-bred normal Beagle. All dogs were part of the breeding colony at the General Animal Research Facility, National Institute of Neuroscience, National Center of Neurology and Psychiatry (Tokyo, Japan), or the Chugai Research Institute for Medical Science, Inc. (Nagano, Japan). Ages, body weights, and serum creatine kinase values at the time of MRI of each dog are shown in Table 1. This study was carried out according to the guidelines provided by the Ethics Committee for the Treatment of Middle-sized Laboratory Animals of the National Center of Neurology and Psychiatry (Approval Nos. 18-02, 19-02, and 20-02).

MR Scanning and Image Analysis. General anesthesia was induced by an intravenous injection of thiopental sodium (20 mg/kg) before MRI scanning and was maintained by inhalation of isoflurane (2.0–3.0%). We examined lower leg muscles of these dogs by superconducting 3.0-Tesla MRI (Magnetom Trio; Siemens Medical Solutions, Erlangen, Germany) with a human extremity coil 18 cm in diameter. The MRI pulse sequences used were T1-weighted imaging (T1WI), T2WI, chemical shift selective T1-weighted imaging (CHESS-T1WI), CHESS-T2WI, gadolinium-enhanced T1-weighted imaging (Gd-T1WI), chemical shift selective gadolinium-enhanced T1-weighted imaging (CHESS-

Table 1. Clinical profiles of normal and dystrophic male dogs used in this study.

	Age (mo)	BW (kg)	Serum CK (IU/L)
Normal dogs			
II-2308MN	3	6.8	197
II/III-3911MN	3	7.7	318
II-4202MN	3	5.8	274
00-174MN	87	13.7	83
CXMDJ dogs			
II-2302MA	3	7.2	30,200
II/III-3903MA	3	6.6	22,300
II-4204MA	3	6.0	28,800
II-C04MA	85	11.5	6500
II-C12MA	94	11.6	1602

Body weight (BW) and serum creatine kinase (CK) values were measured on the day of MRI examination.

Gd-T1WI), and multi-echo T2WI for calculation of T2 relaxation time. In contrast-enhanced images, we injected 0.2 ml/kg of the gadolinium-based MR contrast agent Gd-DTPA (Magnevist; Bayer Schering Pharma, Berlin, Germany) for each sequence. In 3-month-old dogs, we scanned the images for 26 minutes, about 5 minutes after the intravenous injection. On the other hand, we took the images for 13 minutes in 7-year-old dogs at 25 minutes after the injection in order to minimize the risk of anesthesia on the cardiac involvement seen in advanced $CXMD_J$.[15] CHESS was employed to assess necrotic and inflammatory changes more precisely. The acquisition parameters for T1WI, CHESS-T1WI, Gd-T1WI, and CHESS-Gd-T1WI were based on spin echo: repetition time (TR)/echo time (TE) = 500/7.4 ms; slice thickness = 4 mm; field of view = 18 × 18 cm; matrix = 256 × 256; and NEX = 3. The parameters for T2WI and CHESS-T2WI were chosen based on fast spin echo: TR/TE = 4000/85 ms; slice thickness = 4 mm; field of view = 18 × 18 cm; matrix = 256 × 256; turbo-factor = 9; and NEX = 3. The parameters for multi-echo T2WI were selected based on spin echo: TR = 2000; TE = 11.8–118.0 (10 echoes); slice thickness = 4 mm; field of view = 28 × 28 cm; matrix = 256 × 256; and NEX = 2. We were able to clearly distinguish each lower leg muscle by each sequence. Representative cross-sectional images and anatomical locations of lower leg muscles by CHESS-T1WI in a 7-year-old normal dog are shown in Figure 1.

For quantitative analysis of the images, the manufacturer's software (Syngo MR2004A; Siemens Medical Solutions, Erlangen, Germany) was used. Flow artifacts were slight, but regions of interest (ROIs) were selected to avoid flow artifacts and large vessels as follows: three circular ROIs were picked in both right tibialis cranialis (Rt. TC) and extensor digitorum longus (Rt. EDL) muscles of the 3-month-old dogs. ROIs were also selected in the Rt. TC of the 7-year-old dogs and a normal dog. Then, T2 relaxation time or signal intensities (SIs) of CHESS-T1WI, CHESS-Gd-T1WI, and CHESS-T2WI were measured in these ROIs. Signal-to-noise ratios (SNRs) of each ROI were calculated by the equation: SNR = SI/SD_{air}, where SD_{air} was the standard deviation (SD) of background noise.[35] The contrast enhancement (CE) ratio was calculated using the SNR of CHESS-T1WI ($SNR_{precontrast}$) and SNR of CHESS-Gd-T1WI ($SNR_{postcontrast}$) by the following equation: CE = $SNR_{postcontrast}/SNR_{precontrast}$. We used the means of the quantitative values at three points of ROIs for statistical analysis.

Statistical Analysis. The T2 relaxation time, CE ratio, and SNR of CHESS-T2WI were evaluated using a one-way analysis of variance (ANOVA) to determine differences among the groups. When a significant difference was found with one-way ANOVA, intergroup comparisons were undertaken using Fisher's protected least significant difference test. All values are expressed as mean ± SE, and statistical significance was recognized at $P < 0.05$.

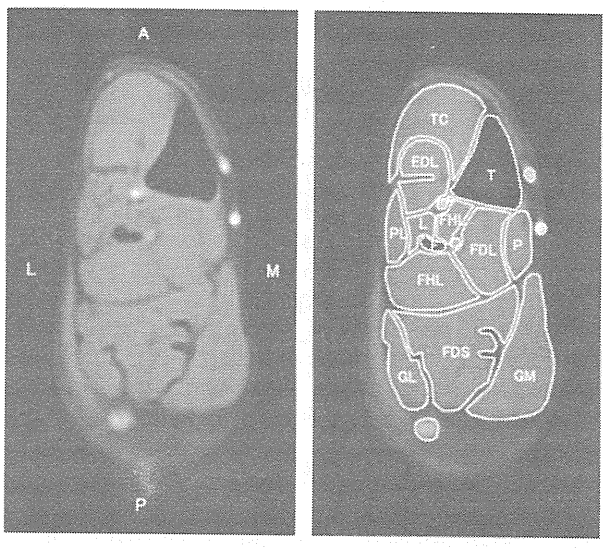

FIGURE 1. Cross-sectional images and anatomical orientation of right lower leg muscles of a 7-year-old normal dog in CHESS-T1WI. A 7-year-old normal dog (00-174MN) was used for this study. T, tibia; F, fibula; TC, tibialis cranialis; EDL, extensor digitorum longus; FHL, flexor hallucis longus; FDL, flexor digitorum longus; FDS, flexor digitorum superficialis; GM, gastrocnemius medialis; GL, gastrocnemius lateralis. A, anterior; P, posterior; L, lateral side; M, medial side.